Mineral-whole rock isotope fidelity? A comparative study of Hf-Nd-O from high Ba Sr granitoids

Emilie Bruand, C. Storey, M. Fowler, B. Dhuime, Régis Doucelance

Mineral-whole rock isotope fidelity? A comparative study of Hf-Nd-O from high Ba-Sr granitoids.

Bruand[1,2], E., Storey[3], C., Fowler[3], M., Dhuime[4], B., Doucelance, R.[1]

[1] Laboratoire Magmas et Volcans, CNRS, Université Clermont Auvergne, France ; [2] Laboratoire Geo-Ocean, CNRS, Université de Bretagne Occidentale, France ; [3] University of Portsmouth, School of Environment, Geography and Geosciences, Portsmouth, UK; [4] CNRS-UMR 5243, Géosciences Montpellier, Université de Montpellier, France

Corresponding author: emilie.bruand@univ-brest.fr
Laboratoire Geo-Ocean
IUEM, Technopôle Brest-Iroise
Rue Dumont d'Urville
29280 PLOUZANE
ORCID ID: 0000-0003-2711-4019

Abstract

It is well-established that lanthanide rare earth elements (REEs) have the potential to record the nature and source characteristics of their host magmas, in both whole-rock and their minerals. Accessory minerals that concentrate REEs are especially useful in crustal evolution studies, both for their elemental and isotopic information; the classic and unrivalled example being zircon. Approaches using a single radiogenic isotopic system, or one radiogenic and one stable isotope system (e.g., Hf and O) in one REE-bearing mineral (usually zircon) are common, but those involving multiple isotopes in several minerals remain scarce despite offering many advantages. Importantly, the latter approaches also allow comparing different techniques and provide evidence on whether isotopic systems were disturbed by secondary processes. This contribution documents several isotopic systems within the abundant accessory mineral of Caledonian high Ba-Sr granitoids from Northwest Scotland. We present a multi-isotope study of titanite, zircon and apatite from two localities (Strontian and Rogart), which were selected for their contrasting whole-rock isotopic signatures - the former deriving from a depleted mantle source, whereas the latter derived from a strongly enriched mantle source. New in-situ Sm-Nd in titanite and apatite and Hf in zircon isotope data are discussed and compared with in-situ

oxygen isotope data previously published for the same samples. An internal consistency is observed for Nd isotopes in apatite and titanite. Nd isotopes values for both minerals strongly correlate with Hf isotopes in zircon. Isotopic data at the mineral scale confirm the Strontian and Rogart source characteristics previously defined from whole-rock isotope data, with the Rogart having a more enriched signature than the Strontian source along the "Caledonian Parental Magma Array"(CPMA). In contrast, a significant discrepancy exists between whole-rock and REE-mineral oxygen isotope data as the latter can be affected by post emplacement alteration and hence can be misinterpreted. Importantly, the contribution of sediments in the CPMA source(s) can be estimated from a diagram combining Sm-Nd isotopic signatures and $(La/Sm)_N$ in apatite and titanite. Overall, we demonstrate that detailed petrogenetic records are not only available in zircons but also in magmatic titanite and apatite, and we suggest that integrated multi-mineral approaches have potential to maximise constraints from in-situ mineral isotope geochemistry.

Keywords: Nd isotopes, Hf isotopes, O isotopes, titanite, apatite, zircon, high Ba-Sr granitoids, magma petrogenesis.

1. Introduction

Advances in analysing various isotope systems in accessory minerals at (sub)-mineral scale have been critical in improving our understanding of the geological processes that shaped the continental crust. For example zircon ($ZrSiO_4$), by way of U-Pb geochronology coupled with radiogenic Hf and stable O isotopes, has provided tight constraints on crust formation processes up to 4.4 billions years ago in the Hadean (e.g. Wilde et al. 2001a; Bell et al. 2011). Isotopic data in zircon also greatly improved our knowledge of the mechanisms and rates of crustal growth, by linking sedimentary and igneous records (e.g. Kemp et al. 2007; Belousova et al. 2010; Dhuime et al. 2012). However, there is increasing evidence that by studying zircon only, we are limiting our ability to fully understand a number of geological processes. This is mostly because (i) zircon crystallization is biased toward felsic compositions and (ii) when studying the complex history of ancient terrains, zircon is not very sensitive to important secondary processes, such as metamorphism or metasomatism (Fisher et al. 2019; Hammerli et al. 2019). More recently, significant progress has been made with less studied REE-minerals (e.g. titanite, apatite, monazite, allanite), and it is now possible to interrogate multiple accessory minerals

(including zircon) within a given rock. For example, trace elements in REE-minerals record petrogenetic information about granite petrogenesis (e.g., mixing, crystal fractionation; e.g. Miles et al. 2013; Bruand et al. 2014; Laurent et al. 2017). In particular, trace elements in these minerals are sensitive to melt polymerisation (Prowatke and Klemme, 2006, 2005) and hence have potential to constrain the bulk mafic or felsic composition of their host rocks. Strontium concentration in apatite is a good proxy for the whole-rock Sr concentration (Sr_{WR}), and by extrapolation for the SiO_2 content of the magma (e.g., Jennings et al. 2011; Bruand et al. 2016). Other trace elements and halogens can record metasomatic processes (e.g. Harlov, 2015; Zirner et al., 2015). Recent advances with in-situ O isotope analysis have enabled the production of reliable data for a variety of REE-minerals (Bonamici et al., 2014; Bruand et al., 2019; Sun et al., 2016; Wudarska et al., 2020), which can be used to track potential alteration or sediment input to a magma source. Development of Sm-Nd in-situ analysis in various REE-minerals has been widely applied to igneous and metamorphic rocks (e.g. Foster and Vance 2006; Fisher et al. 2011b; Yang et al. 2014; Doucelance et al. 2020). Finally, other in-situ analytical procedures are currently being developed on REE-minerals: for instance Sr isotopes in apatite to trace the source of igneous rocks in the same fashion as Sm-Nd isotopes (Emo et al., 2018; Gillespie et al., 2021). In the context of this burgeoning array of mineral-scale elemental and isotopic new approaches, attention has recently turned to the coherence between mineral and whole-rock data. For example, Gregory et al. (2009) showed that accessory minerals are a faithful proxy for the Sm-Nd isotopic composition of recent calc-alkaline magmas, while Hammerli et al. (2014) quantified the equilibration of the Sm-Nd isotopic system in accessory minerals along a metamorphic gradient. However, a few recent studies have highlighted the decoupling of accessory mineral U-Pb and Sm-Nd isotopes in Archean granitoids. These studies, along with other studies on the decoupling of isotopic systems and/or trace elements in REE-minerals (e.g., Hf, Sr, U-Pb; Antoine et al., 2020; Fisher et al., 2019; Gordon et al., 2021; Hammerli et al., 2019), have important implications for our ability to reconstruct complex ancient terrains, with more work required to better understand the responsible parameters (P, T, fO_2, fluid properties). Approaches using a single isotopic system in one REE-mineral are common, but those involving multiple isotope analyses in several accessory minerals remain scarce (e.g. Fisher et al. 2019). The latter allow cross-calibration of different techniques and provide evidence on whether isotopic systems have been disturbed or not by secondary processes. Here we present a multi-isotopic study on selected REE-minerals from late Caledonian high-Ba-Sr granitoids sampled in Northern Scotland. Our data include new in-situ Sm-Nd isotopes in apatite and titanite, Hf isotopes in zircon, as well as O isotopes previously published by (Bruand et al.,

2019). This represents the most comprehensive dataset of three isotope systems in three accessory minerals and their host rocks. Our approach allows us to rigorously test mineral versus whole-rock isotopic fidelity, and we show that in undeformed Phanerozoic granitoids selected for this study, radiogenic isotope ratios (Hf and Nd) give consistent values in all phases, while there is a notable discrepancy for O isotopes between whole rocks (O_{WR}) and REE-minerals (O_{REEml}). We emphasise that titanite and apatite are, in the same way as zircon, powerful minerals to track magma sources, refine petrogenetic models and overcome late alteration of O_{WR} data.

2. Geological and geochemical setting

All samples presented here are from high Ba-Sr granites intruded at the end of the Caledonian orogeny in Scotland. They have been interpreted as the result of a slab break off (Atherton and Ghani, 2002; Fowler et al., 2008, Archibald et al, 2022) consequent upon continental collision between Laurentia and Baltica that followed closure of Iapetus during the Silurian and Devonian (Atherton and Ghani, 2002; Soper et al., 1992). Geological features relevant to this study are described below but readers can refer to previous papers for the tectono-magmatic evolution of Scottish Highlands granites (e.g. Archibald et al., 2022; Brown et al., 2008; Miles et al., 2016; Soper, 1986; Stephens and Halliday, 1984).

The late Caledonian high Ba-Sr suite intrudes the Northern Highland terrane and can be divided petrographically into a western group of syenites and related rocks and a central-eastern group of granitic plutons and associated appinites (Fig. 1, Fowler et al., 2008 and references therein). In this contribution, we present new isotopic data on REE-bearing minerals (titanite, apatite, zircon) from Rogart and Strontian plutons belonging to the central eastern granitic plutons. We chose these two localities for their contrasting origins from relatively enriched (Rogart) and relatively depleted sources (Strontian) along a "Caledonian Parental Magma Array" (Fowler et al., 2008). The Rogart and Strontian igneous complexes have a broadly concentric geometry and are dominated by biotite-hornblende granodiorite. Strontian has a biotite granodiorite central facies surrounded by hornblende-biotite granodiorite, which grades from porphyritic to non-porphyritic at its margin (Sabine, 1963). The hornblende-biotite granodiorite has been dated at 425 ± 3 Ma (U-Pb on zircon) and 423 ± 3 Ma (U-Pb on titanite; (Rogers and Dunning, 1991). The Rogart igneous complex is made up of an inner granodiorite and an outer tonalite, which are cross cut by a later granite. It is coeval with Strontian and has been dated around 420 Ma (K-Ar on biotite; Brown et al., 1968) and 425 ± 1.5 Ma (U-Pb on zircon; Kocks et al., 2014).

Appinites (Bailey and Maufe, 1916) are mafic magma bodies (from centimetre to hundreds of metres scale) present in the main facies of both the Strontian and Rogart plutonic bodies. Scottish appinites are hydrous, mantle-derived rocks with shoshonitic affinities (Fowler, 1988; Fowler et al., 2008), and are widely believed to be the plutonic equivalents of calc-alkaline lamprophyres (Murphy, 2013; Rock, 1984). Local mingling and mixing relationships can be observed between the main plutonic facies and the appinitic bodies in both plutons (Stephenson, 1999). A mingling and intimate mixing event is recorded in the chemistry of apatite and titanite from the Strontian granite samples (Bruand et al., 2014). On the basis of elemental, stable and radiogenic isotope evidence, both plutons are believed to have evolved by fractional crystallisation concurrent with variable assimilation of the surrounding Moine metasediments (Fowler et al., 2001, 2008).

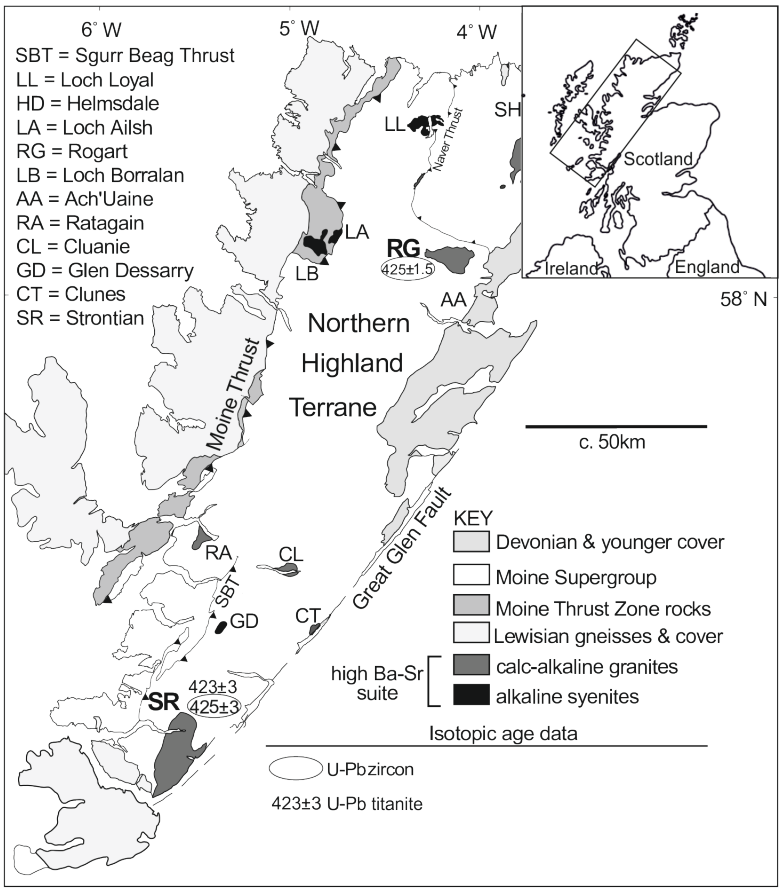

Figure 1: Map from the Northern Highland region (Scotland), modified after Fowler et al. (2008) and showing samples localities and ages from Rogers and Dunning (1991), Brown et al. (1968) and (Kocks et al., 2014)**. RG (Rogart) and SR (Strontian) granites localities are the focus of this study.**

3. Sample selection and preparation

Eight samples were selected for this study: three hornblende-biotite (hb-bi) granodiorites (SR1, SR3, SR4) and one appinite (SR2) from Strontian; as well as two tonalites (RT1, R2), one granite (RHG1) and one appinite (RA1) from Rogart. All samples from both plutons contain abundant accessory titanite, apatite and zircon (Bruand et al., 2017, 2014). All hb-bi granodiorite samples from Strontian are chemically similar for major and trace element contents while granitoid compositions for major and trace elements contents from Rogart vary more widely. Details on whole rock major and trace elements contents and their interpretation can be found in Fowler et al. (2008) for Strontian and Fowler et al., (2001) for Rogart. Appinites in the central-eastern Northern Highlands carry the high Ba-Sr elemental signature, but are commonly even more enriched in LILEs (e.g. Sr, Ba), HFSEs (e.g. Nb, Th) and transition metals (e.g. Cr, Ni, V) than associated granodiorites and granites (Fowler et al., 2008). These characteristics can be observed in the two appinitic samples studied here (SR2 and RA1).

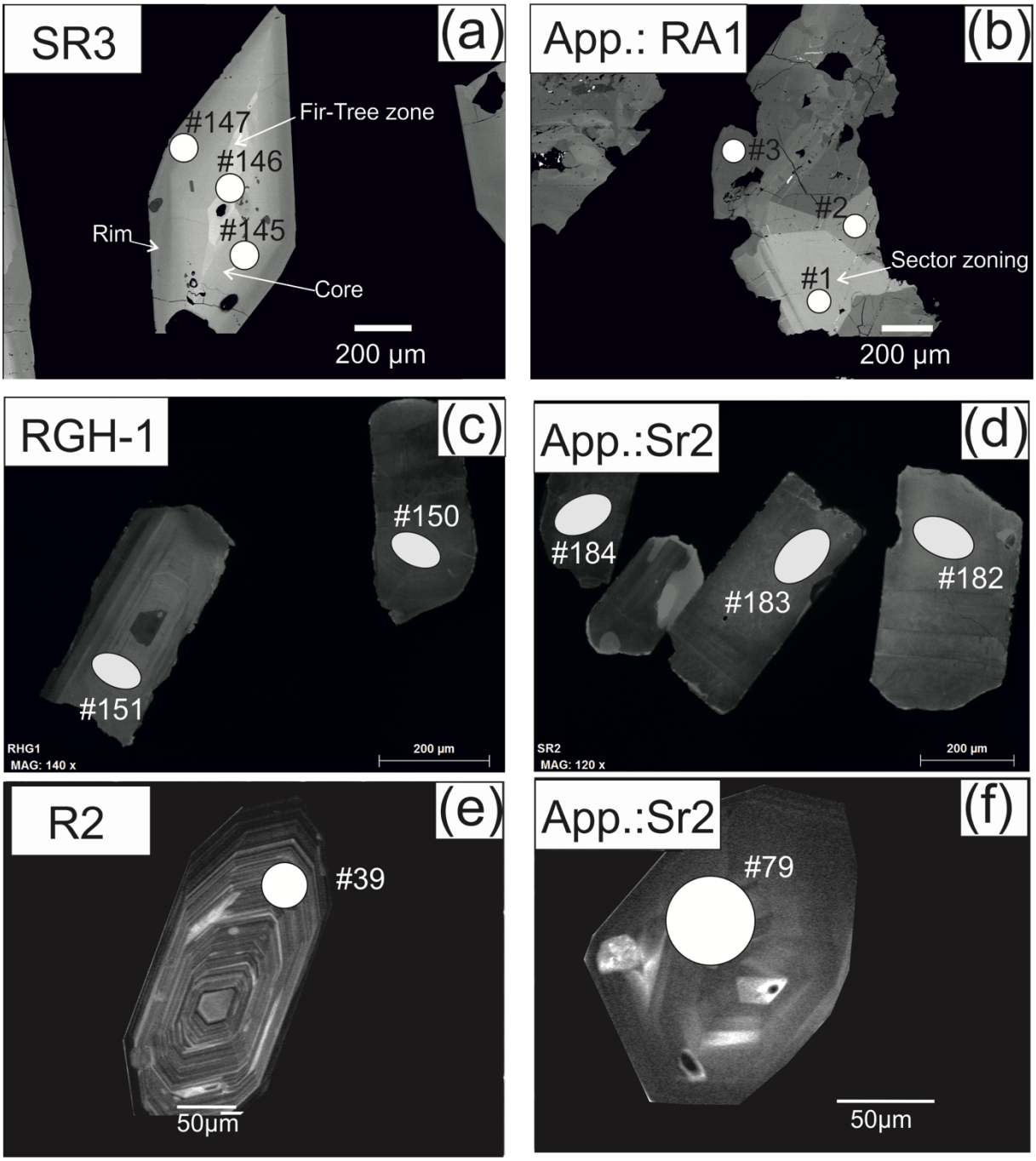

Figure 2 : Representative back-scattered electron images of titanite (a-b). RA1 and SR2 are appinites, other samples are granitoids. (a-d) Numbers represent Nd isotope analyses done by LA-MC-ICPMS and correspond to the data reported in appendix A. (e-f) Numbers represent Hf isotope analyses (Appendix B)

The samples were crushed (jaw-crusher, ball mill or Selfrag™), sieved (<355 µm, 355-500 µm and 500-1000 µm fractions) and passed over a Wilfley table. A diamagnetic separator was then used to obtain fractions of different heavy minerals based on their diamagnetic properties. Titanite, apatite and zircon were handpicked, mounted in epoxy resin discs and polished for in-situ chemical analysis. All accessory minerals studied in the different samples

have been imaged prior to analysis (Figs. 2) and characterised for their major and trace elements chemistries (Bruand et al., 2017, 2014). Further details concerning the studied samples (Whole rock data, petrography and accessory mineral analyses) can be found in Fowler et al. (2008, 2001) and Bruand et al. (2019, 2014), and are not repeated here.

4. Analytical techniques

The following text describes the analytical methods for new data presented herein. Associated O isotope procedures are described in Bruand et al. (2019).

4.1 In-situ Sm-Nd isotope measurements in apatite and titanite

Neodymium isotope measurements were performed using a Thermo Fisher Scientific™ Neptune Plus™ mass spectrometer coupled with a 193-nm wavelength Resonetics™ M-50E laser system at the Laboratoire Magmas et Volcans (LMV, Clermont-Ferrand, France). Analyses were realised with a combination of X-Skimmer and Jet-interface cones and followed the procedure described in Doucelance et al. (2020). For titanite, typical measurements consisted of 70 or 90 cycles with a laser ablation spots of 73 μm in diameter. For apatite, raster analyses were performed (53 μm spot size, 85 μm length) with 130 cycles and an integration time of 1s. The same spot/raster settings were applied on the standards. The first 15 cycles being of every measurement were used to evaluate the baseline level of each Faraday Cup. Oxides were monitored and maintained at <5% (ThO/Th). Baseline and gain reductions were operated online; all other calculations were performed off-line using an in-house Microsoft Excel™ spreadsheet. Gain calibration was done at the beginning of each analytical session. Analyses were performed over 5 different analytical sessions. Doped-Jndi glass was analysed regularly during the different sessions to monitor potential $^{147}Sm/^{144}Nd$ drift that has been reported previously (Doucelance et al., 2020). Primary standards for apatite (Durango from Doucelance et al., 2020; $^{143}Nd/^{144}Nd$= 0.512483 and $^{147}Sm/^{144}Nd$= 0.076096) and titanite (SPREN; $^{143}Nd/^{144}Nd$= 0.512252 and $^{147}Sm/^{144}Nd$= 0.1319 or MKED-1; $^{143}Nd/^{144}Nd$= 0.51163 and $^{147}Sm/^{144}Nd$= 0.127 ; Foster and Vance, 2006; Spandler et al., 2016) have been used for normalization and to correct for instrumental drift when necessary. Laser fluence was set to 3.8-4.1 J/cm^2, frequency 6 Hz, He flow rate was 700-875 ml/min and N_2 1.8-2.6 ml/min depending on the session. All unknowns and standards data acquired can be found in Supplementary data_Table 1. Initial εNd values were calculated using the decay constant of

$6.54*10^{-12}$ (Lugmair and Marti, 1978), the CHUR parameters of $^{143}Nd/^{144}Nd$ =0.512630 and $^{147}Sm/^{144}Nd$ =0.1960 (Bouvier et al., 2008) and an age of 425 Ma for the samples from both localities.

4.2 In-situ Lu-Hf isotope measurements in zircon

The Lu-Hf analyses were performed at the University of Bristol (Bristol Isotope Group) using a ThermoFinnigan Neptune plus multicollector inductively-coupled plasma mass spectrometer (MC-ICP-MS) coupled with a Photon-Machine Analyte G2 Excimer laser (193 nm wavelength). Ablation was performed using 50 μm and 40 μm spot sizes, a laser frequency of 4 Hz, and the energy density of the laser beam was c. 6 J/cm^2. A typical analysis was 90 seconds, including a 30 seconds background measurement and a 60 seconds ablation period. Correction for the interferences and mass bias followed the Bristol routine procedure (Hawkesworth and Kemp, 2006; Kemp et al., 2009). The correction for the isobaric interference of Yb and Lu on ^{176}Hf was made following a method detailed in Fisher et al. (2011a). For Yb, the interference-free ^{171}Yb was corrected for mass bias effects using an exponential law and $^{173}Yb/^{171}Yb$ = 1.132685 (Chu et al., 2002). The mass bias-corrected ^{171}Yb was monitored during the run and the magnitude of the ^{176}Yb interference on ^{176}Hf was calculated using $^{176}Yb/^{171}Yb$ = 0.901864 (Chu et al., 2002). For Lu, the interference-free ^{175}Lu was corrected for mass bias effects assuming βLu = βYb and using an exponential law. The mass bias-corrected ^{176}Lu was monitored during the run and the magnitude of the ^{176}Lu interference on ^{176}Hf was calculated using $^{176}Lu/^{175}Lu$ = 0.02655 (Vervoort et al., 2004). Interference-corrected $^{176}Hf/^{177}Hf$ were corrected for mass bias using an exponential law and $^{179}Hf/^{177}Hf$ = 0.7325 (Patchett and Tatsumoto, 1981), and were finally normalized to JMC-475 = 0.282160. The accuracy and long-term reproducibility of the measurements were gauged by analysing repeatedly three zircon reference standards (Plesovice, Mud Tank and TEMORA 2; Supplementary data_Table 2). $^{176}Lu/^{177}Hf$ vs $^{176}Yb/^{177}Hf$ values of our unknowns plot within the range of standards analysed during analytical session attesting to efficient isobaric correction. Initial ε_{Hf} values for this study were calculated using the decay constant of $1.867*10^{-11}$ (Söderlund et al., 2004), the CHUR parameters $^{176}Hf/^{177}Hf$=0.282785 and $^{176}Lu/^{177}Hf$ = 0.0336 (Bouvier et al., 2008) and an age of 425 Ma.

5. Results

Full data are available in Appendix A, and a summary that also includes published O isotope data is presented in Table 1 below.

Table 1 : Summary of isotopic data for the studied samples. *Whole rock isotopic analyses are from Fowler et al. (2001, 2008). Reported whole rock uncertainties are based on uncertainties of the standards analysed during the analytical session. The values reported are averages and associated standard deviations for each sample. β Oxygen data are from Bruand et al. (2019). εHf , $^{87}Sr/^{86}Sr_i$ and εNd are calculated at 425 Ma.

	Sample	RA1	RT1	R2	RGH1	SR1	SR2	SR3	SR4
		appinite	tonalite	tonalite	granite	granodiorite	appinite	granodiorite	granodiorite
Whole rock*	**εNd**	-0.3	-4.1	-3.9	-	0.7	0.1	0.3	1.4
	2SD	0.5	0.5	0.5	-	0.5	0.5	0.5	0.5
	$^{87}Sr/^{86}Sr_i$	0.70630	0.70633	0.70673	-	0.70527	0.70577	0.70559	0.70559
	2SD	0.00002	0.00002	0.00002	-	0.00002	0.00002	0.00002	0.00002
	$\delta^{18}O$	-	8.5	8.7	-	8	6.7	7.8	6.7
	2SD	-	0.2	0.2	-	0.2	0.2	0.2	0.2
Zircon	**Av. εHf**	-	-5.6	-5.9	-5.7	-0.8	-1.7	-0.3	-2.3
	2SD	-	1.2	1.1	0.8	1.2	1.4	1.4	1.2
	Av. $\delta^{18}O_\beta$	5.6	6.2	5.9	6.0	6.0	5.9	5.7	6.3
	2SD	0.3	0.5	0.7	0.3	0.3	0.4	0.4	0.2
Titanite	**Av. $\delta^{18}O_\beta$**	4.3	4.8	4.7	5.2	4.8	5.4	5.3	4.3
	2SD	0.7	0.4	0.2	0.4	0.8	0.3	0.3	0.3
	Av. εNd	-1.0	-3.8	-4.2	-4.3	0.9	-0.2	0.8	0.4
	2SD	0.8	0.7	0.7	0.7	0.6	1.0	1.2	0.8
Apatite	**Av. $\delta^{18}O_\beta$**	5.1	5.3	5.3	5.8	-	6.1	5.8	4.6
	2SD	0.4	0.4	0.3	0.4	-	0.6	0.5	0.7
	Av. εNd	-0.4	-3.7	-3.7	-4.2	-	0.0	1.2	0.7
	2SD	1.0	0.9	1.7	2.1	-	1.9	2.0	2.1

5.1 Sm-Nd isotopes in apatite and titanite.

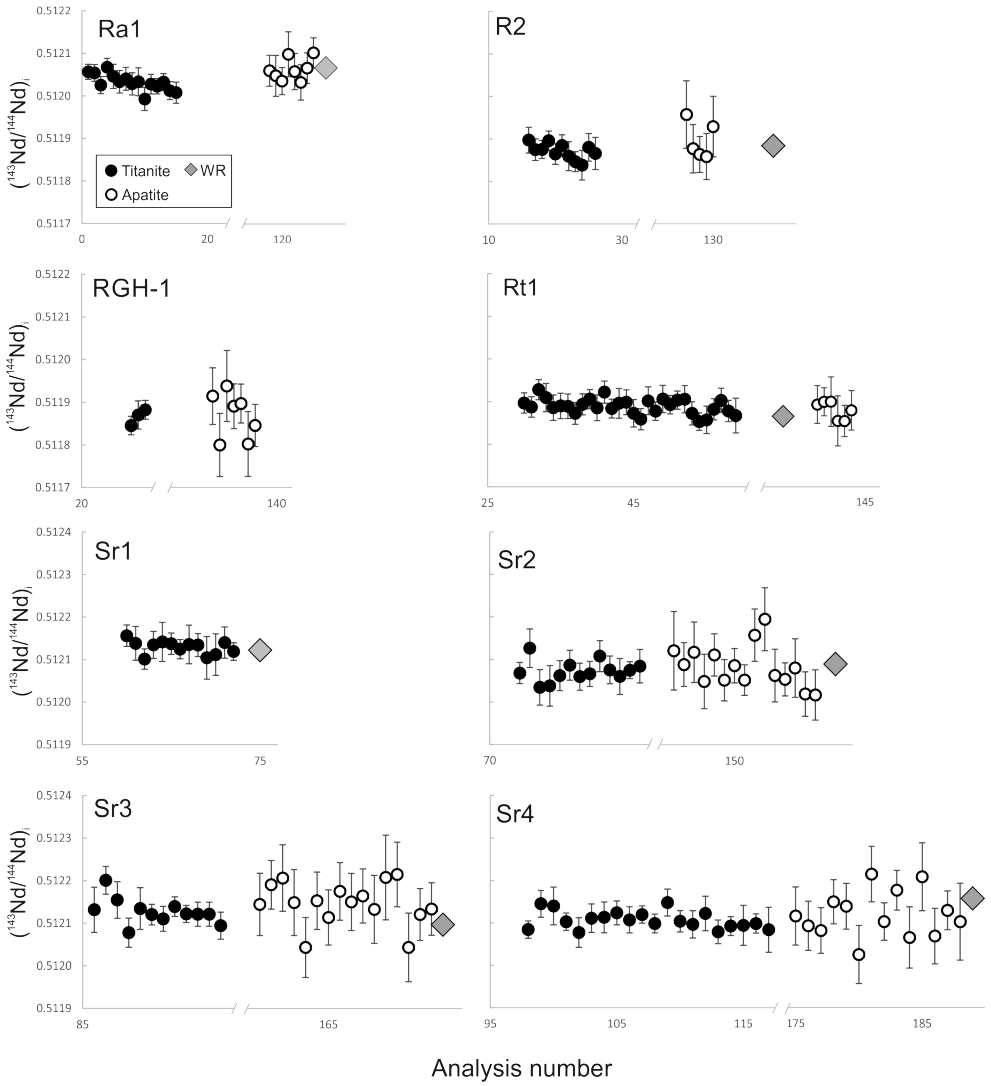

Figure 3 : $^{143}Nd/^{144}Nd_{initial}$ for apatite and titanite from both localities (R = Rogart and S = Strontian), along with whole rock (WR) data from the same samples (Fowler et al. , 2001 and 2008). Error bars on single minerals and whole rock are 2 sigma and are smaller than symbols if not visible. Dashed horizontal lines represents whole rock value.

Overall, Nd isotope data for the high Ba-Sr samples can be split into two groups. The first group includes Rogart samples RT1, R2 and RGH-1 with similar average $^{143}Nd/^{144}Nd_i$ values ranging between 0.511866 (±0.000038; 2SD) and 0.511889 (±0.000036) for titanite, and between 0.511870 (±0.000109) and 0.511896 (±0.000087) for apatite (Fig. 3 and Appendix_A). The second group includes all Strontian samples + Rogart appinite RA1, with similar average $^{143}Nd/^{144}Nd_i$ values ranging between 0.512032 (±0.000039) and 0.512129 (2SD 0.000032) for titanite, and 0.512083 (±0.000083) and 0.512119 (±0.000109) for apatite (Fig. 3 and Appendix_A). Most data are within uncertainty of the whole-rock associated (Fig. 3). Average εNd_i values for group 1 samples are reported in Table 1. They are between -3.8 ± 0.8 (2SD) and

-4.3 ± 0.8 (2SD) for titanite and between -3. 7 ± 1.8 (2SD) and -4.20 ± 2.1 (2SD) for apatite. For group 2 Strontian samples and RA1, average εNd_i values are between -1.0 ± 0.8 (2SD) and 0.9 ± 0.6 (2SD) for titanite and -0.4 ± 1.0 (2SD) and 1.2 ± 2.0 (2SD) for apatite.

Rogart apatite and titanite $^{143}Nd/^{144}Nd_{initial}$ values are identical within uncertainty (Fig. 3). Overall, due to their lower concentration in LREE and the smaller spot required for analyses, errors on apatite analyses are greater than for titanite. For example, Nd concentrations in titanite from RA1 vary between 5300 and 11900 ppm, but between 762 and 1700 ppm for apatite (Bruand et al., 2014). Such differences are present in all samples studied here (Bruand et al., 2014). Consequently, reproducibility on RA1 titanite $^{143/144}Nd_i$ is 76 ppm and 102 ppm on apatite (Appendix_A). For the same reasons, greater errors for apatite measurements are also observed in Strontian samples. For example, uncertainty on SR3 titanite is 120 ppm, but 200 ppm on apatite (Appendix_A).

5.2 Lu-Hf isotopes in zircon

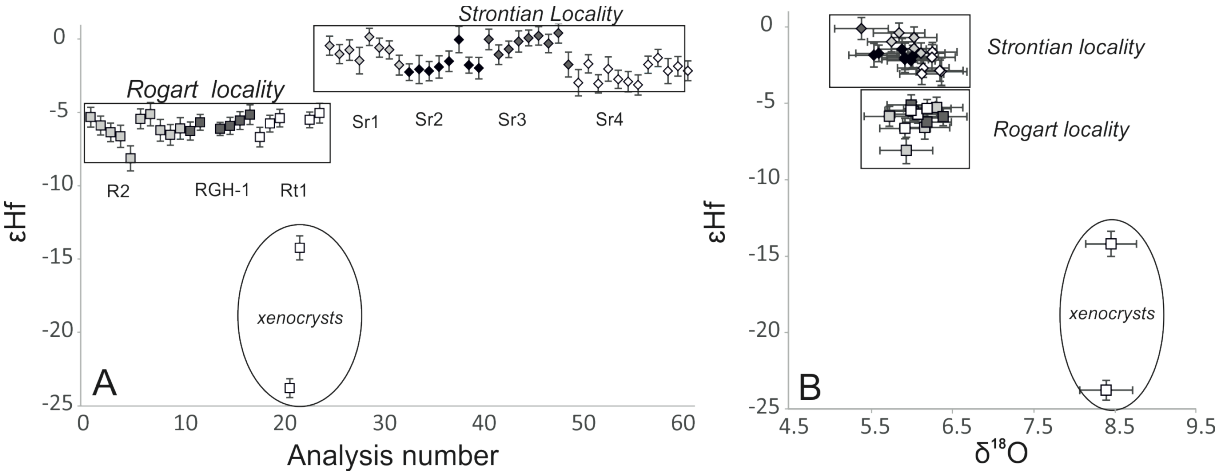

Figure 4 : εHf (A; this study) and $\delta^{18}O$ (B; from Bruand et al. (2019)) in zircon for both localities. Error bars are 2 sigma and are smaller than symbols if not visible.

Hf isotopes have been measured in all samples except RA1 which is an appinite with very few zircons. Those separated were analysed for trace elements and oxygen isotopes but attempts with Hf led to unacceptable signal due to the presence of inclusions during ablation. The remaining data define the same two analytical groups (Fig. 4A). Rogart granitoids (R2, RGH-1, RT1) have average εHf ranging between -5.9 ± 0.6 (1SD) and -5.7 ± 0.6 (1SD), whilst a more radiogenic group defined by Strontian samples vary between -2.3 ± 0.6 (1SD) and -0.3 ± 0.7 (1SD; Table 1 and Appendix_B). Two data points from RT1 are not included in the average calculations. They have very negative εHf (-23.8, -14.2) measured in xenocrystic cores (Fig. 4,

Appendix_B). These xenocrysts have not been dated and reported εHf values have been calculated at 425 Ma for the sake of comparison.

6. Discussion

First we discuss the results for minerals, which are less commonly analysed for their available isotope systems - apatite and titanite. We then add data for zircon and consider the potential for enhanced understanding of geological processes with a combined, multi-mineral approach.

6.1 Apatite and titanite versus whole-rock data.

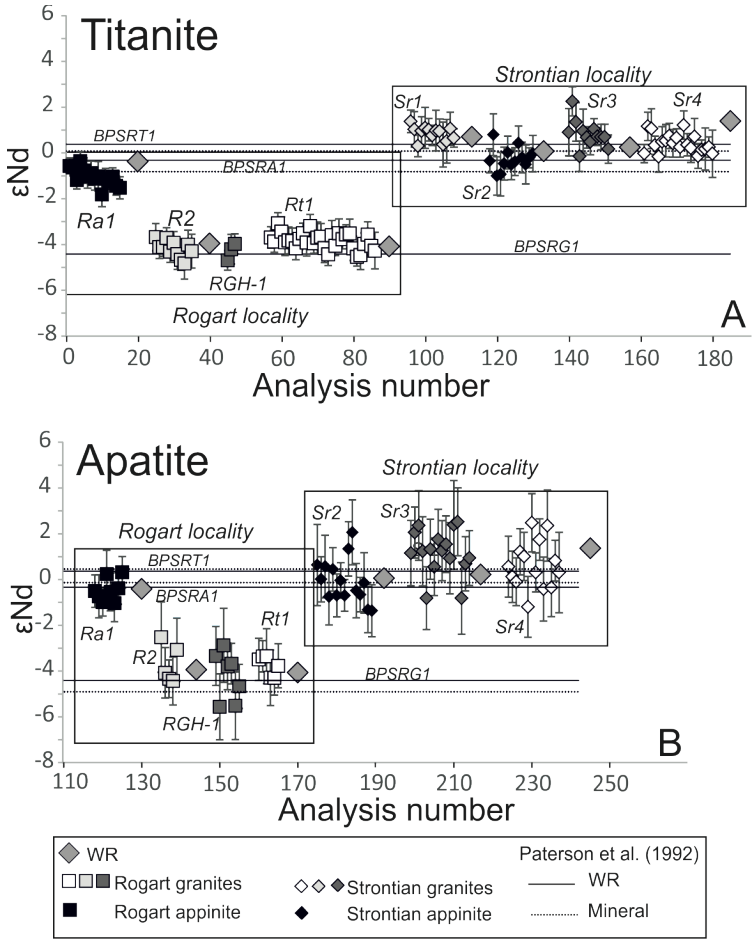

Figure 5 : $\varepsilon Nd_{initial}$ values for titanite (left) and apatite (right) for both localities. Error bars are 2 sigma or within the symbol if not visible. app.= appinite, gr.= granitoid. Black (WR) and dotted lines (a- titanite and b- apatite) are data from Paterson et al. (1992). BPSRT1, BPSRA1 and BPSRG1 are samples from Paterson et al. (1992).

Detailed pioneer work was carried out by Paterson et al. (1992) on different granitoid samples from Strontian. They presented Sm-Nd isotopic analyses for both whole-rocks and fractions of multiple grains (apatite, titanite, +/- monazite and zircon). They obtained an εNd_{WR} of 0.4 (±1.2, 2SD), εNd_{ap} -0.1 (±1.2, 2SD), $\varepsilon Nd_{titanite}$ 0.1 (±0.8, 2SD) for Strontian granodiorite (BPSRT1), and they reported εNd values for one sample in the center of the pluton with an εNd_{WR} value of -4.4 (±0.8, 2SD) (cf. Table 1). These results are in line with our new data (Figure 5). Interestingly, Paterson et al. (1992) also reported Sm-Nd analyses in zircon in disequilibrium with the other accessory phases (titanite, monazite) and the whole-rocks, and they concluded to a potential inherited contribution from some zircons. Over the last three decades, the development of in-situ techniques has allowed to analyse smaller zones of single minerals with better uncertainties, to refine (i) our understanding of chemical and isotopic behaviour of accessory minerals and (ii) petrogenetic processes affecting magmas. Our new data reveal a close consistency between εNd in apatite and titanite within the same sample and, importantly, with previous whole-rock determinations (Table 1). As highlighted in Section 5, εNd values obtained in Rogart granites (RT1, R2 and RGH-1) are similar and range between -3.8 and -4.3 for titanites, and between -3.7 and -4.2 for apatite (Table 1), while the appinitic sample from the same locality (RA1) give higher εNd values for titanite (about -1.0) and for apatite (about -0.4). Overall, this last sample is comparable with εNd from Strontian (Fig. 5). Appinitic samples from both localities tend to have slightly lower titanite average εNd (-0.2 for SR2 and -1.0 for RA1, Table 1) than for Strontian granitoids (εNd=0.4-0.9, Fig. 5A). This is however not fully resolvable considering uncertainties on the data. While more scattered, apatites show exactly the same tendency (Fig. 5B). When disaggregated by locality, some familiar differences emerge (Fig. 5). On the basis of whole-rock data isotopes only, Fowler et al. (2008) argued that the parent magmas of the high Ba-Sr granitoids derived from a Caledonian Parental Magma Array (CPMA, Fig. 6b) that extended from isotopically depleted to isotopically enriched compositions, broadly from the southwest toward the northeast of the Northern Highland Terrane (Fig. 1). A number of high Ba-Sr granites, including Strontian and Rogart, fall on well-defined εNd vs $^{87}Sr/^{86}Sr_i$ trajectories suggesting assimilation of host rock Moine metasediments, from either end of the CPMA (Fig. 6b). For Rogart, Fowler et al. (2001) proposed that AFC was the controlling process and that the isotopic values limited Moine input to ca. 25%. Later, Fowler et al. (2008) suggested that Strontian evolved via similar processes but originated from less-enriched mantle-derived parent magmas. One key observation that the

most mafic samples were often the most "contaminated" is confirmed by our RA1 appinite in-situ data (Fig. 5). This was interpreted as the consequence of a complex building of the plutonic body involving several batches of magma with different routes within the crust.

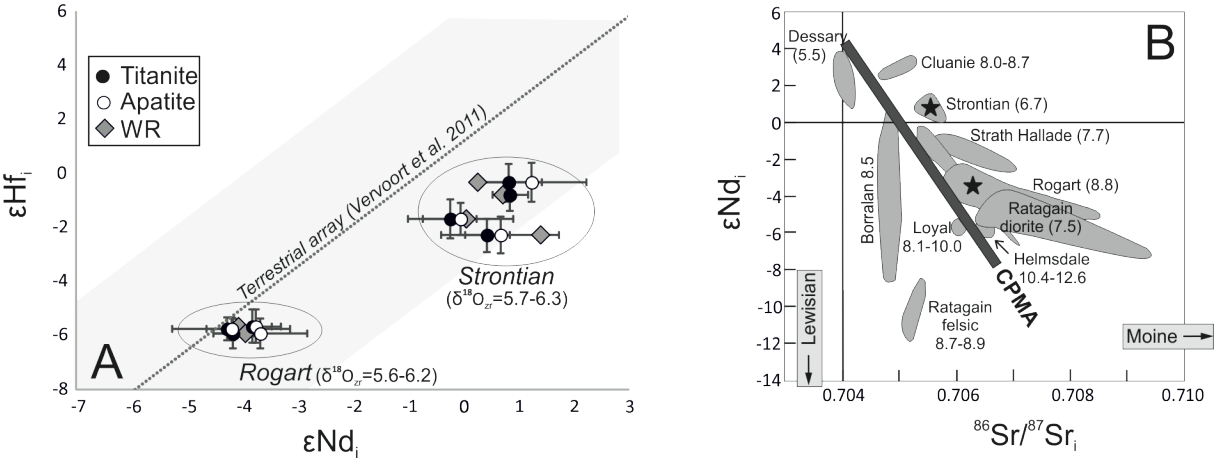

Figure 6: A- $\varepsilon Nd_{initial}$ for titanite, apatite and WR versus $\varepsilon Hf_{initial}$ in zircon for Rogart and Strontian localities. $\delta^{18}O_{zr}$ ranges are also reported on the figure. Appinite RA1 sample is not reported on this figure due to the lack of Hf data. Error bars are 1 SD. B- from Fowler et al. (2001): εNd versus $^{87}Sr/^{86}Sr_i$ for Caledonian high Ba-Sr granitoids from the NHT including Strontian and Rogart (black stars), annotated with $\delta^{18}O_{WR}$. CPMA= Caledonian Parental Magma Array.

In contrast to the fidelity with which radiogenic isotopes in accessory minerals record the primary composition of the source magma from which they crystallised, the oxygen signature is not so clear cut. Fowler et al (2008) observed higher whole-rock O isotope values for Rogart ($\delta^{18}O$ =8.5-10.6‰) than for Strontian ($\delta^{18}O$=6.7-8‰, Fig. 7), apparently correlated with increasing $^{86}Sr/^{87}Sr_i$ and decreasing εNd (Fig. 6b) and unrelated to LOI (Fowler et al., 2008, their Fig. 10). These were originally interpreted as the consequence of higher pelagic sediment input to the Rogart mantle source (Fowler et al., 2008). A subsequent study of the same samples using in-situ O isotopes in accessory minerals (Bruand et al., 2019 – the source of the O data considered here) recorded homogeneous oxygen isotopes across all minerals (apatite, titanite and zircon) from both localities (Fig. 7). This decoupling between whole rock and in-situ oxygen data was interpreted as the consequence of feldspar alteration (visible in thin section), being stronger in Rogart and in the most differentiated samples (Bruand et al., 2019). The petrogenetic consequence is that required pelagic sediments input previously estimated at about 10% for these samples is not a preferred model anymore (Fowler et al., 2008).

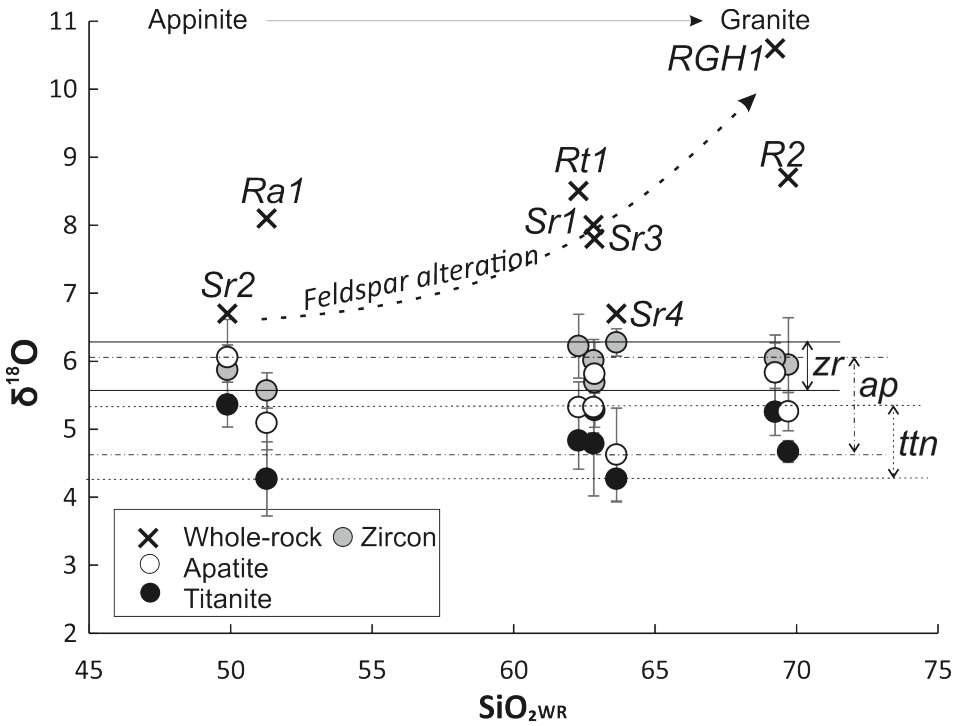

Figure 7: δ ^{18}O versus SiO_{2WR} for high Ba-Sr samples modified after Brand et al. (2019).). RHG1 has a higher δ ^{18}O whole-rock value (10.6 ‰), which is interpreted to be the result of late feldspar alteration (Fowler et al., 2001; Bruand et al., 2014). No variations of oxygen isotopic values are resolvable between the less and the most differentiated samples for apatite and titanite. zr: zircon, ap: apatite, ttn: titanite.

6.2 Hf in zircon vs Sm-Nd in apatite and titanite.

The Hf and Nd isotope systems are very closely related, an obvious result of their parentage. Plotting average εHf in zircon versus εNd in titanite and apatite for both localities plot close to the terrestrial array (Fig. 6a). The datasets reveal two groups of samples – Rogart and Strontian, relatively "enriched" and "depleted" respectively in both isotope systems, directly comparable with the traditional whole-rock treatment of Nd and Sr isotopes (Fig. 6b). Both diagrams illustrate that the juvenile component increase from Rogart to Strontian. Strontian samples are plotting slightly lower than the terrestrial array line itself but is still within the original field defined by the data in Vervoort et al. (2011, grey field on figure 6a). These slightly lower values, could also be interpreted as the consequence of residual xenocrysts preventing the full homogeneisation of the magma source during the incorporation of rocks rich in zircons. Both localities present xenocrysts but dissolution of zircon in the magma source might have been less efficient than in Rogart.

6.3 Tracking sediment/crustal assimilation by combining isotopes and elements in apatite and titanite

Mineral chemical data gathered from the same accessory minerals (Bruand et al, 2014, 2020) provide the opportunity to investigate variations in elemental ratios that are key for petrogenetic studies. Earlier studies have demonstrated the potential of using REE-bearing minerals and the Sm-Nd systems in crustal evolution studies (Fisher et al., 2017; Gregory et al., 2009; Hammerli and Kemp, 2021). In particular, Gregory et al. (2009) have shown that in-situ Nd isotopes in REE-minerals could faithfully record the source characteristics of a suite of plutons in the Bergell pluton (Italy). Later, Hammerli et al., (2018) used a combination of Nd-Hf-O isotopes in accessory minerals and whole rock to trace melt source in the crust. Although the Nd signature of the magma source was very successfully recovered, they failed to find trace elements systematics tracking crustal assimilation. From the present dataset, we provide an index of crustal assimilation, which is given by the $(La/Sm)_N$ ratio. The $(La/Sm)_N$ ratio in apatite has been shown sensitive to the Aluminium Saturation Index (ASI) of igneous rocks (e.g. Belousova et al., 2001; Bruand et al., 2020; Miles et al., 2013), with apatite from peraluminous magmas (ASI>1) having lower $(La/Sm)_N$ ratios than apatite from metaluminous magmas (ASI<1). In the present sample suite, all studied samples are metaluminous, but $(La/Sm)_N$ variations reveal interesting features seemingly related to the source of the studied granitoids. In figure 8, the $(La/Sm)_N$ versus εNd for apatite and titanite shows consistent differences between the plutons - positive εNd (ca. 0.5) with relatively high $(La/Sm)_N$ (up to 7.8 in titanite and 20 in apatite) at Strontian versus negative εNd (ca. -4) with relatively low $(La/Sm)_N$ (between 0.5 and 2.3 in titanite and <5 in apatite) at Rogart. Part of the $(La/Sm)_N$ variation observed within accessories in a given sample has been attributed to in-situ crystal fractionation (Bruand et al. 2014). Additionally, part of this scatter within a given sample can also occasionally reflect competition with other accessory phases and/or delay of crystallization of certain phases. For example, titanite (interstitial in texture) is crystallising late in the appinites while apatite is crystallising early. Even if the scatter of data is relatively pronounced in each sample, there is a clear difference between the 2 granitoid localities that cannot account for in-situ crystal fractionation. This interpretation is confirmed by whole rock data as both localities have similar whole rock SiO_2-MgO ranges and have been shown to have encountered similar crystallization fractionation process (Fowler et al., 2001, 2008). Whole rock $(La/Sm)_N$ for both granitoids localities have a similar range and show no correlations with εNd.

In their whole-rock study, Fowler et al. (2008) defined a "Caledonian Parental Mantle Array" as a variable source for Scottish Caledonian granitoids (Fig. 6b), defined by variable sediment input in the source. In this study, we show that the variations of up to 5 εNd recorded between both localities in both phases are clearly recording the influence in sediments along the Caledonian Parental Magma Array previously defined as the main reservoir of Caledonian granitoids in Northwest Scotland (Fig 8b). On the other hand, $\delta^{18}O_{zr}$ in the same samples show limited variations (5.6-6.3 ‰, Table 1) close to a mantle-like source ($\delta^{18}O_{zrmantle}$=5.3±0.6 2SD, Valley and Kita, 2009). The maximum estimated AFC contamination (based on radiogenic isotopes) is of the order of 25% (Fowler et al., 2001). On the other hand, the maximum estimated Moine metasediment input into the source, using an average Moine $\delta^{18}O$ value of about 8‰ to attain the maximum $\delta^{18}O$ of our sample, is about 15%. This interesting discrepancy is currently unresolved, but could perhaps relate to fractionation from incongruent dynamic melting reactions during assimilation, a sample spot bias towards early-crystallising zones in the accessory phases or be related to the analytical uncertaintie. Using Sr isotopes, Fowler et al. (2008) could distinguish two clear sources of subsequent crustal contamination moving the granitoids signatures away from the CPMA: (i) Moine metasediment contamination affecting the granites (e.g., Rogart, Strontian) and (ii) Lewisian basement contamination affecting the syenites (Fig. 6b). Based on whole rock isotope data, both localities sampled here have been affected by Moine metasediments assimilation, which created small εNd variations (< 3 εNd; Fowler et al., 2008).

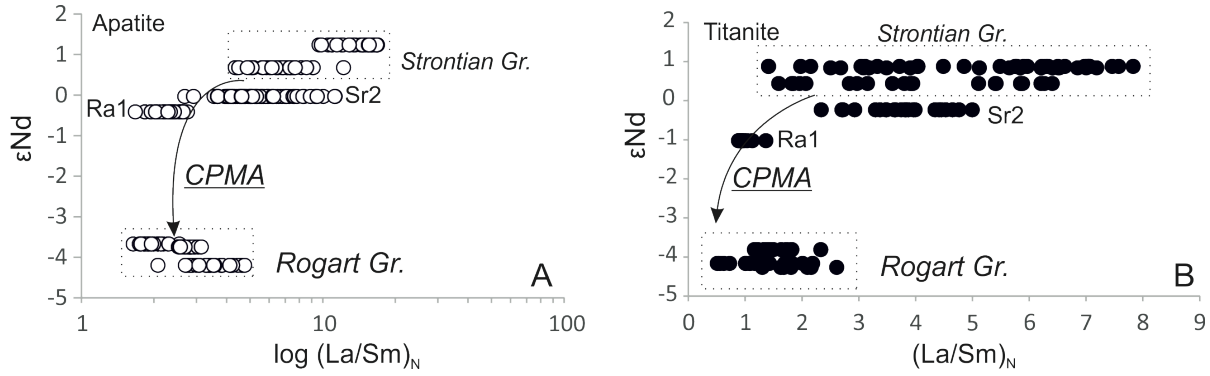

Figure 8: $\varepsilon Nd_{initial}$ versus log $(La/Sm)_N$ in apatite (A) and titanite (B) for both localities. $\varepsilon Nd_{initial}$ values are averages values per samples (Table 1) and $(La/Sm)_N$ are from Bruand et al. (2014, 2020). Ra1 and Sr2 are appinites while Rogart Gr. and Strontian Gr. are granitoids. CPMA= Caledonian Parental Magma Array. Both minerals record the influence of the CPMA source in their elemental and isotopic signatures. Trace elements data are from Bruand et al. (2014) and can be found in Appendix_C.

Gregory et al. (2009) and Sun et al. (2021) reported internal variation of εNd within apatite, interpreted as evidence of local crustal assimilation preserved at the grain scale. To our knowledge, there are no such reports using titanite. In our case, confirmation of at least some crustal assimilation is provided by the presence of xenocrysts in zircons. Thus, while trace element chemistry in zircon from granitoids is less amenable to petrogenetic interpretation, its well-known capacity to preserve xenocrysts can add important additional constraints. In both locations reported here, xenocrysts in zircon have been described (Bruand et al., 2014). Unfortunately, Hf measurements could be performed only in one sample (from Rogart). εHf results for two xenocrysts are strongly negative and may suggest contamination with a strongly enriched component (Fig. 4b). As the xenocryst could not be dated, the εHf values are minimum values. Oxygen isotope measurements ($\delta^{18}O$ up to 8.5‰) are consistent with this interpretation. Other xenocrysts have been analysed for O but not Hf isotopes, due to their small size. They range between 5.9‰ and 8.7‰, which is a slightly larger variation than that observed in the granites (5.5-6.5‰; Bruand et al., 2019). Very few literature data combining O and Hf measurements exist for the local Moine metasediments, but two samples in the Morar formation analysed by Lancaster et al. (2011) show similar values to the xenocrysts of this study.

6.4. Implication for ancient terranes

Earlier studies (e.g. Iizuka et al., 2011) have proved that Sm-Nd isotopes in accessory minerals constitute the only robust record of the evolution of the Sm-Nd system in eroded or disturbed ancient terranes. However, accessory minerals in granitoids can also be reactive to metamorphism. They may record past metamorphic events under certain conditions: (i) a temperature above the closure temperature of the accessory mineral has to be attained; (ii) whole-rock characteristics and/or fluid-assisted metamorphic event can promote their dissolution and reprecipitation (e.g. Rapp and Watson, 1986; Watson, 1996; Wolf and London, 1994).

As a consequence, metamorphic events affecting ancient terranes have potential to reopen isotopic systems in accessory minerals, and to erase their primary igneous history leading to anomalous whole-rock isotopic signatures. This has been recently discussed in two studies on accessory minerals within Archean grey gneisses (Hammerli et al., 2019; Fisher et al., 2020), and this may explain apparent contradictory findings in the recent literature. Indeed, contradictory radiogenic signatures for Hf isotopes in zircon and Nd isotopes in bulk-rock have

been at the core of major speculations about early Earth's evolution. The discovery of super-chondritic Nd isotope ratios was used to infer the presence of a highly depleted mantle early in Earth history, and which could reflect the extraction of large volumes of crust (Bennett et al., 1993). However, chondritic Hf isotope ratios in zircon point towards no/little mantle depletion over the same period of time (Vervoort and Kemp, 2016). Recent measurements (Hammerli *et* al., 2019*)* on accessory minerals from Eoarchean gneisses suggest that these minerals can record LREE mobility during HT metamorphic events that can shift whole-rock Nd radiogenic value. It is important to note that although these studies rely only on few heavily disturbed samples, they highlight several limitations in our current knowledge of the effect of metamorphism on LREE behaviour in accessory phases, which needs to be better addressed in the future. For example in Fisher et al. (2020), while the U-Pb system in apatite dates a younger event from the Slave craton (1.8-1.9 Ga, Wopmay orogeny), its Sm-Nd signature preserves a much older event (at about 2.65 Ga). This observation highlights that the reopening of the U-Pb system could be much more sensible than the Sm-Nd isotopic system. Another key observation in Fisher et al. (2020) is that different accessory minerals can record different timing of the reopening of the Sm-Nd system. Indeed, in Acasta while the apatite Sm-Nd isochron records a 2.65 Ga event, titanite records a much older Sm-Nd signature (3.3 Ga) consistent with zircon U-Pb age. This study (Fisher et al., 2020) is consistent with recent trace elements data collected on apatite and titanite in Archean TTG affected by greenschist to amphibolite facies, which reveal that trace elements in titanite are less prone to be disturbed by metamorphism than in apatite (Bruand et al., 2020). Indeed, Bruand et al. (2020) have demonstrated that trace elements in accessory minerals from Archean granitoids affected by later greenschist to amphibolite facies from different cratons (Kaapvaal, Slave, Karelia) could preserve under certain conditions original/igneous trace elements concentrations. The major impact of metamorphism on titanite and apatite chemistry was demonstrated to induce a decrease of LREE concentration. They could clearly show that in the Slave craton, secondary apatite were depleted in LREE when compared to primary apatite (e.g. apatite inclusions armoured in zircon). Under greenschist to amphibolite facies, the same chemical systematic on apatite chemistry has also been convincingly demonstrated on other lithologies (e.g. metapelite: Henrichs et al., 2018; O'Sullivan et al., 2020). Combining the ability of the Sm-Nd system to date the geological process recorded, its source tracer potential and trace element signatures within the accessory phases, give new opportunities to refine geological event affecting igneous rocks (e.g. later metamorphic event, mixing event with another magma, etc.). Once the igneous origin of the accessory minerals have been confirmed using recent trace elements discriminators (e.g.

O'Sullivan et al., 2020; Bruand et al., 2020), the εNd associated to element ratios such as $(La/Sm)_N$ in apatite or titanite could help to refine the source characteristics of a given magma (Fig. 8). Ultimately this will allow to observe the crustal/sediment component in its source at the grain scale.

7 Conclusion

In this contribution we document several isotope systems within zircon, apatite and titanite. We show close agreement between radiogenic isotopes (Hf and Nd) within the accessory minerals and with previous whole rock data (Nd) to confirm an unbiased radiogenic isotope record in the accessory phases. A main point of this study being that while Nd isotopes and associated $(La/Sm)_N$ in apatite and titanite are powerful indicator of the CPMA source variabilities present in the northwest Scotland Caledonian granites, the assimilation of the host Moine sediments is only clearly visible by the presence of xenocrysts in zircons.

Acknowledgements

We are grateful to M. Gannoun for the help provided with the LA-MC-ICPMS analyses. This work was partly supported by the Natural Environment Research Council (grant NE/I025573/1), by the French Government Laboratory of Excellence initiative n° ANR-10-LABX-0006, and by the French National Research Agency (grant ANR-21-CE49-0001-01, AMNESIA, PI EB). This is Laboratory of Excellence ClerVolc contribution number 586. This manuscript benefited from constructive reviews by two anonymous reviewers. We thank Balz Kamber for his editorial handling.

References

Antoine, C., Bruand, E., Guitreau, M., Devidal, J.-L., 2020. Understanding Preservation of Primary Signatures in Apatite by Comparing Matrix and Zircon - Hosted Crystals From the Eoarchean Acasta Gneiss Complex (Canada). Geochemistry, Geophysics, Geosystems 1–21. https://doi.org/10.1029/2020GC008923

Archibald, D.B., Murphy, J.B., Fowler, M., Strachan, R.A., Hildebrand, R.S., 2022. Testing petrogenetic models for contemporaneous mafic and felsic to intermediate magmatism within the "Newer Granite" suite of the Scottish and Irish Caledonides. New Developments in the Appalachian-Caledonian-Variscan Orogen. https://doi.org/10.1130/2021.2554(15)

549 Atherton, M.P., Ghani, A.A., 2002. Slab breakoff: A model for Caledonian, Late Granite syn-
550 collisional magmatism in the orthotectonic (metamorphic) zone of Scotland and
551 Donegal, Ireland. Lithos 62, 65–85. https://doi.org/10.1016/S0024-4937(02)00111-1
552 Bailey, E.B., Maufe, H.B., 1916. The geology of Ben Nevis and Glen Coe and the
553 surrounding country (revised by EB Bailey). Memoirs of the Geological Survey of Great
554 Britain. Edinburgh, Her Majesty's Stationery Office.
555 Bell, E.A., Harrison, T.M., Mcculloch, M.T., Young, E.D., 2011. Early Archean crustal
556 evolution of the Jack Hills Zircon source terrane inferred from Lu – Hf , 207 Pb / 206 Pb
557 , and d 18 O systematics of Jack Hills zircons. Geochim Cosmochim Acta 75, 4816–
558 4829. https://doi.org/10.1016/j.gca.2011.06.007
559 Belousova, E.A., Kostitsyn, Y.A., Griffin, W.L., Begg, G.C., O'Reilly, S.Y., Pearson, N.J.,
560 2010. The growth of the continental crust: Constraints from zircon Hf-isotope data.
561 Lithos 119, 457–466. https://doi.org/10.1016/j.lithos.2010.07.024
562 Belousova, E.A., Walters, S., Griffin, W.L., O'Reilly, S.Y., 2001. Trace-element signatures of
563 apatites in granitoids from the Mt Isa Inlier, Northwestern Queensland. Australian
564 Journal of Earth Sciences 48, 603–619. https://doi.org/10.1046/j.1440-
565 0952.2001.00879.x
566 Bennett, V.C., Nutman, A.P., Mcculloch, M.T., 1993. Nd isotopic evidence for transient ,
567 highly depleted mantle reservoirs in the early history of the Earth. Earth Planet Sci Lett
568 119, 299–317.
569 Bonamici, C.E., Kozdon, R., Ushikubo, T., Valley, J.W., 2014. Intragrain oxygen isotope
570 zoning in titanite by SIMS: Cooling rates and fluid infiltration along the Carthage-Colton
571 Mylonite Zone, Adirondack Mountains, NY, USA. Journal of Metamorphic Geology 32,
572 71–92. https://doi.org/10.1111/jmg.12059
573 Bouvier, A., Vervoort, J.D., Patchett, P.J., 2008. The Lu-Hf and Sm-Nd isotopic composition
574 of CHUR: Constraints from unequilibrated chondrites and implications for the bulk
575 composition of terrestrial planets. Earth Planet Sci Lett 273, 48–57.
576 https://doi.org/10.1016/j.epsl.2008.06.010
577 Brown, P.E., Miller, J.A., Grasty, R.L., 1968. Isotopic ages of late Caledonian granitic
578 intrusions in the British Isles. Proceedings of the Yorkshire Geological Society 36, 251–
579 276.
580 Brown, P.E., Ryan, P.D., Soper, N.J., Woodcock, N.H., 2008. The Newer Granite problem
581 revisited: a transtensional origin for the Early Devonian trans-suture suite. Geol Mag
582 145, 235–256.
583 Bruand, E., Fowler, M., Storey, C., Darling, J., 2017. Apatite trace element and isotope
584 applications to petrogenesis and provenance. American Mineralogist 102.
585 https://doi.org/10.2138/am-2017-5744
586 Bruand, E., Fowler, M., Storey, C., Laurent, O., Antoine, C., Guitreau, M., Heilimo, E.,
587 Nebel, O., 2020. Accessory mineral constraints on crustal evolution: elemental
588 fingerprints for magma discrimination. Geochemical Perspectives Letters .
589 https://doi.org/http://dx.doi.org/10.7185/geochemlet.2006
590 Bruand, E., Storey, C., Fowler, M., 2016. An apatite for progress: Inclusions in zircon and
591 titanite constrain petrogenesis and provenance. Geology 44.
592 https://doi.org/10.1130/G37301.1
593 Bruand, E., Storey, C., Fowler, M., 2014. Accessory mineral chemistry of high Ba-Sr granites
594 from Northern Scotland: Constraints on petrogenesis and records of whole-rock
595 Signature. Journal of Petrology 55. https://doi.org/10.1093/petrology/egu037
596 Bruand, E., Storey, C., Fowler, M., Heilimo, E., 2019. Oxygen isotopes in titanite and apatite
597 , and their potential for crustal evolution research. Geochim Cosmochim Acta 255, 144–
598 162. https://doi.org/10.1016/j.gca.2019.04.002

599 Chu, N.C., Taylor, R.N., Chavagnac, V., Nesbitt, R.W., Boella, R.M., Milton, J.A., German,
600 C.R., Bayon, G., Burton, K., 2002. Hf isotope ratio analysis using multi-collector
601 inductively coupled plasma mass spectrometry: An evaluation of isobaric interference
602 corrections. J Anal At Spectrom 17, 1567–1574. https://doi.org/10.1039/b206707b
603 Dhuime, B., Hawkesworth, C.J., Cawood, P.A., Storey, C.D., 2012. A Change in the
604 Geodynamics of Continental Growth 3 Billion Years Ago. Science (1979) 335, 1334 LP
605 – 1336.
606 Doucelance, R., Bruand, E., Matte, S., Bosq, C., Auclair, D., Gannoun, A., 2020. In-situ
607 determination of Nd isotope ratios in apatite by LA-MC-ICPMS : Challenges and
608 limitations. Chem Geol 550.
609 Emo, R.B., Smit, M.A., Schmitt, M., Kooijman, E., Scherer, E.E., Sprung, P., Bleeker, W.,
610 Mezger, K., 2018. ScienceDirect Evidence for evolved Hadean crust from Sr isotopes in
611 apatite within Eoarchean zircon from the Acasta Gneiss Complex. Geochim Cosmochim
612 Acta 235, 450–462. https://doi.org/10.1016/j.gca.2018.05.028
613 Fisher, C.M., Bauer, A.M., Vervoort, J.D., 2020. Disturbances in the Sm – Nd isotope system
614 of the Acasta Gneiss Complex — Implications for the Nd isotope record of the early
615 Earth. Earth Planet Sci Lett 530, 115900.
616 Fisher, C.M., Hanchar, J.M., Miller, C.F., Phillips, S., Vervoort, J.D., Whitehouse, M.J.,
617 2017. Combining Nd isotopes in monazite and Hf isotopes in zircon to understand
618 complex open-system processes in granitic magmas. Geology 45, 267–270.
619 https://doi.org/10.1130/G38458.1
620 Fisher, C.M., Hanchar, J.M., Samson, S.D., Dhuime, B., Blichert-Toft, J., Vervoort, J.D.,
621 Lam, R., 2011a. Synthetic zircon doped with hafnium and rare earth elements: A
622 reference material for in situ hafnium isotope analysis. Chem Geol 286, 32–47.
623 https://doi.org/10.1016/j.chemgeo.2011.04.013
624 Fisher, C.M., McFarlane, C.R.M., Hanchar, J.M., Schmitz, M.D., Sylvester, P.J., Lam, R.,
625 Longerich, H.P., 2011b. Sm-Nd isotope systematics by laser ablation-multicollector-
626 inductively coupled plasma mass spectrometry: Methods and potential natural and
627 synthetic reference materials. Chem Geol 284, 1–20.
628 https://doi.org/10.1016/j.chemgeo.2011.01.012
629 Foster, G.L., Vance, D., 2006. In situ Nd isotopic analysis of geological materials by laser
630 ablation 288–296. https://doi.org/10.1039/b513945g
631 Fowler, M.B., 1988. Elemental evidence for crustal contamination of mantle-derived
632 Caledonian syenite by metasediment anatexis and magma mixing. Chem Geol 69, 1–16.
633 https://doi.org/10.1016/0009-2541(88)90154-4
634 FOWLER, M.B., HENNEY, P.J., DARBYSHIRE, D.P.F., GREENWOOD, P.B., 2001.
635 Petrogenesis of high Ba-Sr granites: the Rogart pluton, Sutherland. J Geol Soc London
636 158, 521–534. https://doi.org/10.1144/jgs.158.3.521
637 Fowler, M.B., Kocks, H., Darbyshire, D.P.F., Greenwood, P.B., 2008. Petrogenesis of high
638 Ba-Sr plutons from the Northern Highlands Terrane of the British Caledonian Province.
639 Lithos 105, 129–148. https://doi.org/10.1016/j.lithos.2008.03.003
640 Gillespie, J., Nemchin, A.A., Kinny, P.D., Martin, L., Aleshin, M., Roberts, M.P., Ireland,
641 T.R., Whitehouse, M.J., Jeon, H., Cavosie, A.J., Kirkland, C.L., 2021. Strontium isotope
642 analysis of apatite via SIMS. Chem Geol 559, 119979.
643 https://doi.org/10.1016/j.chemgeo.2020.119979
644 Gordon, S.M., Kirkland, C.L., Reddy, S.M., Blatchford, H.J., Whitney, D.L., Teyssier, C.,
645 Evans, N.J., McDonald, B.J., 2021. Deformation-enhanced recrystallization of titanite
646 drives decoupling between U-Pb and trace elements. Earth Planet Sci Lett 560, 116810.
647 https://doi.org/10.1016/j.epsl.2021.116810

Gregory, C.J., McFarlane, C.R.M., Hermann, J., Rubatto, D., 2009. Tracing the evolution of calc-alkaline magmas: In-situ Sm-Nd isotope studies of accessory minerals in the Bergell Igneous Complex, Italy. Chem Geol 260, 73–86. https://doi.org/10.1016/j.chemgeo.2008.12.003

Hammerli, J., Kemp, A.I.S., 2021. Combined Hf and Nd isotope microanalysis of co-existing zircon and REE-rich accessory minerals: High resolution insights into crustal processes. Chem Geol 581, 120393. https://doi.org/10.1016/j.chemgeo.2021.120393

Hammerli, J., Kemp, A.I.S., Shimura, T., Vervoort, J.D., Dunkley, D.J., 2018. Generation of I-type granitic rocks by melting of heterogeneous lower crust. Geology 46, 907–910.

Hammerli, J., Kemp, A.I.S., Spandler, C., 2014. Neodymium isotope equilibration during crustal metamorphism revealed by in situ microanalysis of REE-rich accessory minerals. Earth Planet Sci Lett 392, 133–142. https://doi.org/10.1016/j.epsl.2014.02.018

Hammerli, J., Kemp, A.I.S., Whitehouse, M.J., 2019. In situ trace element and Sm-Nd isotope analysis of accessory minerals in an Eoarchean tonalitic gneiss from Greenland : Implications for Hf and Nd isotope decoupling in Earth ' s ancient rocks. Chem Geol 524, 394–405.

Harlov, D.E., 2015. Apatite: A fingerprint for metasomatic processes. Elements 11, 171–176. https://doi.org/10.2113/gselements.11.3.171

Hawkesworth, C.J., Kemp, A.I.S., 2006. Using hafnium and oxygen isotopes in zircons to unravel the record of crustal evolution. Chem Geol 226, 144–162. https://doi.org/10.1016/j.chemgeo.2005.09.018

Henrichs, I.A., Sullivan, G.O., Chew, D.M., Mark, C., Babechuk, M.G., Mckenna, C., Emo, R., 2018. The trace element and U-Pb systematics of metamorphic apatite. Chem Geol 483, 218–238. https://doi.org/10.1016/j.chemgeo.2017.12.031

Iizuka, T., Nebel, O., McCulloch, M.T., 2011. Tracing the provenance and recrystallization processes of the Earth's oldest detritus at Mt. Narryer and Jack Hills, Western Australia: An in situ Sm-Nd isotopic study of monazite. Earth Planet Sci Lett 308, 350–358. https://doi.org/10.1016/j.epsl.2011.06.006

Jennings, E.S., Marschall, H.R., Hawkesworth, C.J., Storey, C.D., 2011. Characterization of magma from inclusions in zircon: Apatite and biotite work well, feldspar less so. Geology 39, 863–866. https://doi.org/10.1130/G32037.1

Kemp, A.I.S., Foster, G.L., Scherstén, A., Whitehouse, M.J., Darling, J., Storey, C., 2009. Concurrent Pb–Hf isotope analysis of zircon by laser ablation multi-collector ICP-MS, with implications for the crustal evolution of Greenland and the Himalayas. Chem Geol 261, 244–260.

Kemp, A.I.S., Hawkesworth, C.J., Foster, G.L., Paterson, B.A., Woodhead, J.D., Hergt, J.M., Gray, C.M., Whitehouse, M.J., 2007. Magmatic and Crustal Differentiation History of Granitic Rocks from Hf-O Isotopes in Zircon. Science (1979) 315, 980 LP – 983.

KOCKS, H., STRACHAN, R., EVANS, J., FOWLER, M., 2014. Contrasting magma emplacement mechanisms within the Rogart igneous complex, NW Scotland, record the switch from regional contraction to strike-slip during the Caledonian orogeny. , 151(5), . Geol Mag 151, 899–915.

Lancaster, P.J., Storey, C.D., Hawkesworth, C.J., Dhuime, B., 2011. Understanding the roles of crustal growth and preservation in the detrital zircon record. Earth Planet Sci Lett 305, 405–412. https://doi.org/10.1016/j.epsl.2011.03.022

Laurent, O., Zeh, A., Gerdes, A., Villaros, A., 2017. How do granitoid magmas mix with each other ? Insights from textures , trace element and Sr – Nd isotopic composition of apatite and titanite from the Matok pluton (South Africa). https://doi.org/10.1007/s00410-017-1398-1

Lugmair, G.W., Marti, K., 1978. Lunar initial 143Nd/144Nd: Differential evolution of the lunar crust and mantle. Earth Planet Sci Lett 39, 349–357. https://doi.org/https://doi.org/10.1016/0012-821X(78)90021-3

Miles, A.J., Graham, C.M., Hawkesworth, C.J., Gillespie, M.R., Hinton, R.W., 2013. Evidence for distinct stages of magma history recorded by the compositions of accessory apatite and zircon. Contributions to Mineralogy and Petrology 166, 1–19. https://doi.org/10.1007/s00410-013-0862-9

Miles, A.J., Woodcock, N.H., Hawkesworth, C.J., 2016. Tectonic controls on post-subduction granite genesis and emplacement: The late Caledonian suite of Britain and Ireland. Gondwana Research 39, 250–260. https://doi.org/10.1016/j.gr.2016.02.006

Murphy, J.B., 2013. Appinite suites: A record of the role of water in the genesis, transport, emplacement and crystallization of magma. Earth Sci Rev 119, 35–59.

O'Sullivan, G., Chew, D., Kenny, G., Henrichs, I., Mulligan, D., 2020. The trace element composition of apatite and its application to detrital provenance studies. Earth Sci Rev 201, 103044. https://doi.org/10.1016/j.earscirev.2019.103044

Patchett, P.J., Tatsumoto, M., 1981. A routine high-precision method for Lu-Hf isotope geochemistry and chronology. Contributions to Mineralogy and Petrology 75, 263–267.

Paterson, B.A., Rogers, G., Stephens, W.E., 1992. Evidence for inherited S m - Nd isotopes in granitoid zircons 378–390.

Prowatke, S., Klemme, S., 2006. Trace element partitioning between apatite and silicate melts. Geochim Cosmochim Acta 70, 4513–4527. https://doi.org/10.1016/j.gca.2006.06.162

Prowatke, S., Klemme, S., 2005. Effect of melt composition on the partitioning of trace elements between titanite and silicate melt. Geochim Cosmochim Acta 69, 695–709. https://doi.org/10.1016/j.gca.2004.06.037

Rapp, R.P., Watson, E.B., 1986. Monazite solubility and dissolution kinetics : implications for the thorium and light rare earth chemistry of felsic magmas. Contributions to Mineralogy and Petrology 94, 304–316.

Rock, N.M.S., 1984. Nature and origin of calc-alkaline lamprophyres: minettes, vogesites, kersantites and spessartites. Earth Environ Sci Trans R Soc Edinb 74, 193–227.

Rogers, G., Dunning, G.R., 1991. Geochronology of appinitic and related granitic magmatism in the W Highlands of Scotland: constraints on the timing of transcurrent fault movement. J Geol Soc London 148, 17–27.

Sabine, P.A., 1963. The Strontian granite complex, Argyllshire. Bulletin of the Geological Survey of Great Britain 20, 6–42.

Söderlund, U., Patchett, P.J., Vervoort, J.D., Isachsen, C.E., 2004. The 176Lu decay constant determined by Lu–Hf and U–Pb isotope systematics of Precambrian mafic intrusions. Earth Planet Sci Lett 219, 311–324.

Soper, N.J., 1986. The Newer Granite problem: a geotectonic view. Geol Mag 123, 227–236.

Soper, N.J., England, R.W., Snyder, D.B., Ryan, P.D., 1992. The Iapetus suture zone in England, Scotland and eastern Ireland: a reconciliation of geological and deep seismic data. J Geol Soc London 149, 697–700.

Spandler, C., Hammerli, J., Sha, P., Hilbert-Wolf, H., Hu, Y., Roberts, E., Schmitz, M., 2016. MKED1: A new titanite standard for in situ analysis of Sm-Nd isotopes and U-Pb geochronology. Chem Geol 425, 110–126. https://doi.org/10.1016/j.chemgeo.2016.01.002

Stephens, W.E., Halliday, A.N., 1984. Geochemical contrasts between late Caledonian granitoid plutons of northern, central and southern Scotland. Earth Environ Sci Trans R Soc Edinb 75, 259–273.

Stephenson, D., 1999. Caledonian igneous rocks of Great Britain. Joint Nature Conservation Committee.

Sun, J.-F., Yang, J.-H., Zhang, J.-H., Yang, Y.-H., Zhu, Y.-S., 2021. Apatite geochemical and SrNd isotopic insights into granitoid petrogenesis. Chem Geol 566, 120104. https://doi.org/https://doi.org/10.1016/j.chemgeo.2021.120104

Sun, Y., Wiedenbeck, M., Joachimski, M.M., Beier, C., Kemner, F., Weinzierl, C., 2016. Chemical and oxygen isotope composition of gem-quality apatites : Implications for oxygen isotope reference materials for secondary ion mass spectrometry (SIMS). Chem Geol 440, 164–178. https://doi.org/10.1016/j.chemgeo.2016.07.013

Valley, J.W., Kita, N.T., 2009. In-situ oxygen isotope geochemistry by Ion Microprobe. Mineralogical Association of Canada Short Course 41, 19–63.

Vervoort, J.D., Kemp, A.I.S., 2016. Clarifying the zircon Hf isotope record of crust – mantle evolution. Chem Geol 425, 65–75. https://doi.org/10.1016/j.chemgeo.2016.01.023

Vervoort, J.D., Patehett, P.J., Söderlund, U., Baker, M., 2004. Isotopic composition of Yb and the determination of Lu concentrations and Lu/Hf ratios by isotope dilution using MC-ICPMS. Geochemistry, Geophysics, Geosystems 5. https://doi.org/10.1029/2004GC000721

Watson, E.B., 1996. Dissolution, growth and survival of zircons during crustal fusion: kinetic principals, geological models and implications for isotopic inheritance. Trans R Soc Edinb Earth Sci 87.

Wilde, S. a, Valley, J.W., Peck, W.H., Graham, C.M., 2001. Evidence from detrital zircons for the existence of continental crust and oceans on the Earth 4.4 Gyr ago. Nature 409, 175–178. https://doi.org/10.1038/35051550

Wolf, M.B., London, D., 1994. Apatite dissolution into peraluminous haplogranitic melts : An experimental study of solubilities and mechanisms. Geochim Cosmochim Acta 58, 4127–4145.

Wudarska, A., Wiedenbeck, M., Słaby, E., Harris, C., Joachimski, M.M., Lécuyer, C., MacLeod, K.G., Pack, A., Vennemann, T., Couffignal, F., Glodny, J., Kusebauch, C., Lempart, M., Sun, Y., Wilke, F., 2020. SIMS- and IRMS-based study of apatite reference materials reveals new analytical challenges for oxygen isotope analysis, in: EGU General Assembly Conference Abstracts, EGU General Assembly Conference Abstracts. p. 18841.

Yang, Y.-H., Wu, F.-Y., Yang, J.-H., Chew, D.M., Xie, L.-W., Chu, Z.-Y., Zhang, Y.-B., Huang, C., 2014. Sr and Nd isotopic compositions of apatite reference materials used in U–Th–Pb geochronology. Chem Geol 385, 35–55. https://doi.org/10.1016/j.chemgeo.2014.07.012

Zirner, A.L.K., Marks, M.A.W., Wenzel, T., Jacob, D.E., Markl, G., 2015. Rare earth elements in apatite as a monitor of magmatic and metasomatic processes: The Il??maussaq complex, South Greenland. Lithos 228–229, 12–22. https://doi.org/10.1016/j.lithos.2015.04.013